Can Tho University Journal of Science
website: ctujs.ctu.edu.vn

DOI: 10.22144/ctu.jen.2022.005

Fabrication of PZT Thick Film by Electrophoretic Deposition on the Platinum Substrate

Ngo Truong Ngoc Mai[1*], Iasmi Sterianou[2], Ian Reaney[3], Luong Huynh Vu Thanh[1], Cao Luu Ngoc Hanh[1] and Dang Huynh Giao[1]

[1]*College of Engineering Technology, Can Tho University, Viet Nam*
[2]*Department of Engineering and Mathematics, Sheffield Hallam University, UK*
[3]*Department of Materials Science and Engineering, University of Sheffield, UK*
**Correspondence: Ngo Truong Ngoc Mai (email: ntnmai@ctu.edu.vn)*

Article info.

Received 29 Sep 2021
Revised 05 Oct 2021
Accepted 22 Nov 2021

Keywords

Electrophoretic deposition, piezoelectrics, Pt substrate, PZT, thick film

ABSTRACT

$PbZr_xTi_{1-x}O_3$ compositions near morphotropic phase boundary have been reported to have high piezoelectric properties. In this study, $Pb(Zr_{0.5}Ti_{0.5})O_3$ (PZT 50/50) powder was produced by the solid-state reaction from the relevant oxides at 950°C. Phase analysis using X-ray diffraction revealed the single phase of the tetragonal perovskite structure. PZT thick film was fabricated by electrophoretic deposition of the resulted PZT powder onto the Pt substrate. The electrophoretic deposition process was conducted in an ethanol medium, and the effects of deposition parameters such as pH, applied voltage and deposition time on the film thickness were investigated. A green film with a maximum thickness of ~95 µm and sintered film with a maximum thickness of 80±2 µm were prepared. The effects of sintering atmosphere and temperatures on phase transformation and microstructures of PZT film were evaluated using X-ray diffraction and scanning electron microscopy. At room temperature, a PZT film of 68 ± 2 µm thickness has a relative permittivity of 477 ± 13 and ~ 9,500 at T_C = 405°C, showing typical dielectric properties.

1. INTRODUCTION

The field of electroceramics has attracted increasing research interest. Their applications are expanding due to the fabrication of new functional materials and the ability to integrate these functions into one component. The combination of micro-technology and ceramic thick/thin films has resulted in microdevices, e.g., production control, environment monitoring and biotechnology applications (Setter, 2001). Studies have recently shifted away from mono-functionally discrete devices to integrated systems with multifunctional electroceramics, including ferroelectric, piezoelectric, pyroelectric and recently magnetoresistant properties.

Lead zirconate titanate (PZT) is the best-known piezoelectric ceramic that has been studied for more than 50 years. The increasing needs of integrating discrete components and reducing their size continue to promote numerous studies in the fabrication of ceramic, thin and thick films for the applications in microactuators, sensors, smart microdevices and microelectromechanical systems (MEMS) (Kuepper et al., 2002; Hsu et al., 2004).

Lead zirconate titanate $Pb(Zr_xTi_{1-x})O_3$ ($0<x<1$) or PZT, a ferroelectric, is a perovskite structured solid solution series of lead zirconate (PZ) and lead titanate (PT), resulting from the substitution of Zr^{4+} for Ti^{4+}. The piezoelectric properties of PZT

ceramics were first discovered by Jaffe et al. in 1954 (Jaffe et al., 1971). The PZ endmember is orthorhombic, and pure PZ ceramic exhibits antiferroelectricity at room temperature, but it becomes paraelectric above Curie point, T_C = 230°C due to a polymorphic transition from orthorhombic to cubic (Carter & Norton, 2013). The PT endmember was ferroelectric and has a high Curie point, Tc = 495°C at which the tetragonal is transformed to cubic phase (Moulson & Herbert, 2003). The substitution of Zr^{4+} for Ti^{4+} in $PbTiO_3$ structure reduces the tetragonal distortion, and a transformation into ferroelectric rhombohedral occurs at the composition termed PZT 53/47 (47 mol% PT) (Jaffe et al., 1971; Moulson & Herbert, 2003; Carter & Norton, 2013).

The fabrication of thick films of PZT can be achieved by several methods, including sol-gel, tape casting, screen printing, sputtering or hydrothermal methods (Mikeska & Cannon, 1988; Hata et al., 1998; Miyazawa et al., 2000; Lee et al., 2002; Piticescu et al., 2004). However, these methods provide too thin films (~ 10 μm) to be applied as a multifunctional material in actuators used in MEMS systems (Doungdaw et al., 2005). Electrophoretic deposition (EPD) is a promising method since it is low cost, fast and suitable for uniform coverage of complex geometries (Ma et al., 2003; Kalinina & Pikalova, 2019; Szklarska et al., 2020). It can be used to manufacture thick films and fiber-reinforced composites and nanostructured materials (Ng & Boccaccini, 2005; Mills et al., 2020; Mittal & Rhee, 2021; Rehman et al., 2021). EPD comprises of electrophoresis and deposition processes. In the electrophoresis process, charged particles in a non-aqueous suspension move toward the electrode under an applied electric field. The deposition occurs when the particles coagulate densely on a metal surface (Sarkar & Nicholson, 1996). For a successful EPD process, the solvent must be non-aqueous and operation parameters must be optimized (Jun & Joo, 2008).

In the context of this study, thick film of PZT 50/50 was produced using EPD processing from a suspension containing ethanol solvent and 3wt% PZT powder synthesized by solid-state reaction. The thickness of the as-deposited films was evaluated at various deposition conditions including powder pH, applied voltage and deposition time. Phase analysis and morphology of the films were characterized. Electrical property of the sintered PZT film was evaluated via relative permittivity and Curie temperature.

2. MATERIALS AND METHOD

2.1. Materials

In this work, lead oxide PbO (99.99%) was purchased from Fisher Scientific, UK; titanium dioxide TiO_2 (99%) and zirconium dioxide ZrO_2 (99%) from Aldrich; Platinum substrate, ethanol, HNO_3, and glacial acetic acid from Alfa Aesar.

2.2. Methods

2.2.1. Preparation of powder PZT

The composition was batched according to the general formulae, $PbZr_xTi_{1-x}O_3$, x = 0.5 using PbO, ZrO_2 and TiO_2 powders as starting oxides. 2 wt% of excess PbO was added to the batch to compensate for the PbO loss due to its volatilization at high temperatures. The oxide powders (molar ratio PbO: ZrO_2:TiO_2 = 1:0.5:0.5) were mixed and ground using an attrition mill. Then, the suspension was separated and dried overnight. The dried agglomerates were passed through a sieve to obtain a fine mixture.

Small amounts of the mixture were calcined for 4 h in lidded crucibles at different temperatures from 700 to 1,000°C. Calcined powders were structurally analyzed by powder X-ray diffraction (XRD) to determine the temperature at which a single phase was formed. The resulting product obtained at chosen calcined temperature was then reground in the attrition mill so that powders of sub-micron size distribution were produced available for electrophoretic deposition.

2.2.2. Electrophoretic deposition of PZT thick films

Figure 1 illustrates a schematic diagram of the EPD experimental set-up. Stainless steel was used as the positive electrode and Pt substrate as the negative electrode for film deposition. A *dc* voltage up to 500 V, 0.6A was generated through a Kikusui regulated DC power supply PAS 500-0.6.

3 g PZT powder was ultrasonically dispersed in the 100 mL ethanol with a concentration of 3% glacial acetic acid. In all experiments, the concentration of PZT in the ethanol suspension was fixed at ~3 wt% due to results from previous studies on agglomeration (Doungdaw et al., 2005; Wu & Vilarinho, 2006). Dilute HNO_3 (1 wt%) solution was slowly added to the suspension to provide electric charges for particle movement to the electrode made from the Pt foil with a surface of 1 cm in diameter. The EPD process was carried out by

varying the pH values of the suspension, the applied voltage and the deposition time.

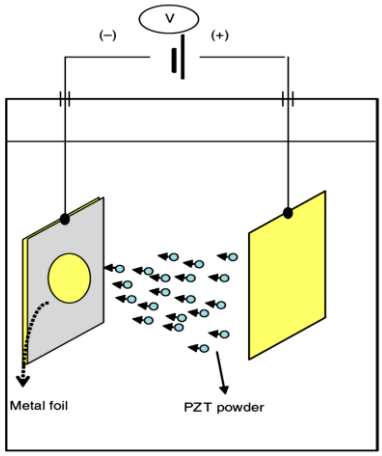

Figure 1. Schematic diagram of the electrophoretic deposition experimental set-up (Wu & Vilarinho, 2006)

2.2.3. Sintering of PZT films

The sintering of PZT films was carried out in a Lenton tube furnace between 1,100 and 1,250°C for 1 h with and without lead-rich powder. The structure and morphology of the films were investigated using XRD and scanning electron microscopy (SEM).

2.2.4. Characterization of PZT powder and thick film samples

Particle sizes of the powder were measured using a Coulter LS130 analyzer. The thickness of the green film was determined with the assumption that the green density would be 60% of the theoretic density (~8.00 g/cm^3) (Wu & Vilarinho, 2006). The thickness of the sintered film was measured using a micrometer.

The phases present in the calcined powders and the sintered films were determined through XRD patterns obtained by the Philips PW1825/00 X-ray diffractometer with a Hiltonbrooks computer controller. The system was operated at 40kV and 30 mA with CuKα1 radiation (λ = 1.54056 Å). SEM images were obtained using a JEM-6400 operating at 20 kV for powder and at 10 kV for the film. The grain compositions were analyzed using an Energy-Dispersive X-ray Spectrometer (EDX) with energy ranging from 10 to 20 kV.

The capacitance C and conductance G of the film were measured on a HP4284a LCR meter over the range of temperature between room temperature and 500°C at a heating rate of 1°C/min. The meter was set to operate at a voltage of 1V and different frequencies between 1 and 1,000 kHz (ω = 10^4 rad/sec). The relative permittivity ε_r and the loss tangent *tanδ* for the film were calculated as follows:

$$\varepsilon_r = \frac{4tC}{\varepsilon_0 \pi d^2} \quad (1)$$

$$\tan\delta = \frac{G}{\omega C} \quad (2)$$

where d and *t* are the diameter and thickness of the film, respectively (m), ε_0 is the permittivity of free space = 8.854x10^{-12} F.m^{-1}.

3. RESULTS AND DISCUSSION

3.1. Preparation and characterization of PZT powders

Below 800°C, the reaction to form PZT is incomplete (not shown). Figure 2 presents the XRD patterns of the powder samples calcined from 800 to 1,000°C in 4 h. The XRD patterns were indexed according to the JCPDS card 70-4057 for $Pb(Zr_{0.5}Ti_{0.5})O_3$ with tetragonal structure. The main characteristic peaks at 2θ = 21.42^0, 22.04^0, 30.92^0, 31.37^0 and 38.3^0 correspond to the planes with *hkl* values (001), (100), (101), (110) and (111), respectively. These values matched well with previous study (Wu & Vilarinho, 2006, Frantti *et al.*, 2000).

The XRD trace of the sample calcined at 800°C shows complete reaction to the PZT phase without detecting excess PbO. However, adjacent peaks due to distortion away from pseudocubic are not well-separated at 800°C. At 900°C, the calcined powder was in loose form showing the sample was not well sintered. Calcination at higher temperatures (>900°C) resulted in well-defined peaks but at higher temperatures than 950°C the calcined powder became a rigid block, which is hard to grind into fine powder. Therefore, a calcination temperature of 950°C was chosen, which gave an XRD trace in which adjacent peaks could be well distinguished, and the calcined powder was easily ground into fine particles to prepare for further processing.

The particle size distribution of PZT powder sintered at 950°C is shown in Figure 3, together with the SEM image. A mean particle size diameter of 1.926 μm was obtained with a noticeable proportion of particles above 2 μm.

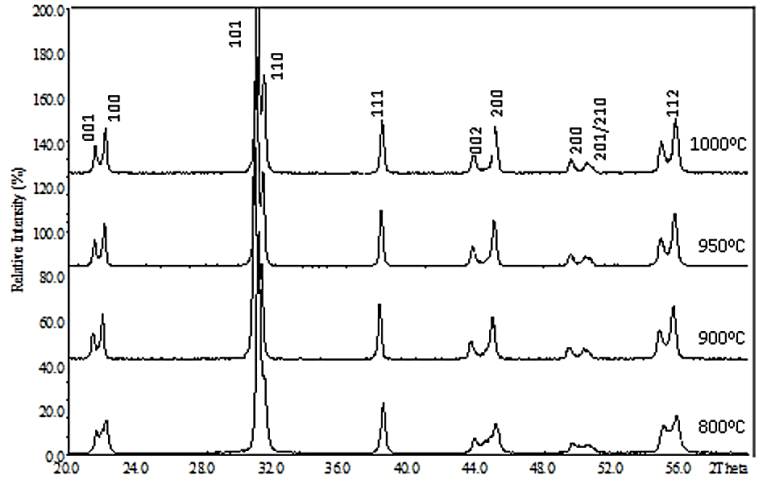

Figure 2. XRD patterns of PZT powders calcined at 800°C, 900°C, 950°C and 1,000°C

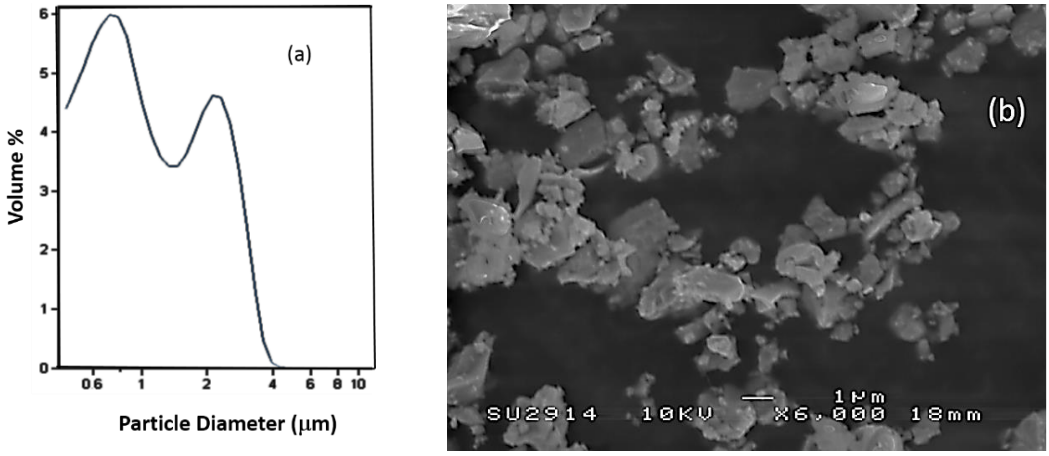

Figure 3. Particle size distribution (a) and SEM image (b) of PZT powder sintered at 950°C, 4 h

3.2. Electrophoretic deposition of PZT thick film

3.2.1. Effect of pH

The electrophoretic deposition was performed under a constant applied voltage of 200 V for 2 minutes to investigate the effect of pH values. Table 1 illustrates the relation of various pH values and film quality. Adding HNO_3 1 wt% to adjust the pH leads to an increase in the Zeta potential and the electrical conductivity of the suspension since more positive charged particles are created and carried to the cathode under an applied field. When the ionic concentration increases too much, *i.e.*, the suspension has low pH, the double layer thickness increases forming large particles depositing on the Pt substrate. As shown in Figure 4a at pH 3.5, the particles agglomerate, resulting in poor microstructure with rough surface of the film. Film becomes smoother when increasing pH. However, in the range of pH from 5 to 6, the film gets thinner since the number of positive particles is reduced.

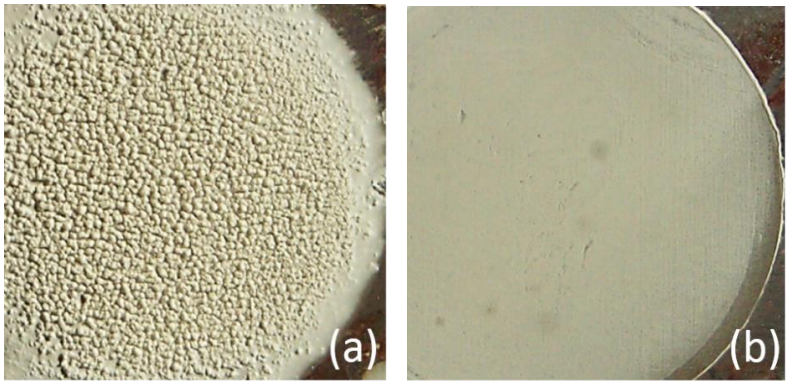

Figure 4. Surface morphology of the films deposited at 200 V, 2 min. and (a) pH 3.5, (b) pH 5

Table 1. Film quality at various pH

pH	Quality of PZT film
< 4	Non-uniform
4-4.5	Uniform
4.5-5	Uniform
5-6	Uniform, thin
> 6.0	No film

When pH is over 6, charge particles fall significantly, and no film was observed. Consequently, an optimum range of pH 4 to 5 exists that the green films can be obtained with high uniformity. This result is consistent with previous study (Ma & Cheng, 2002).

It should be noted that the pH values presented in Table 1 were measured using a pH meter which was calibrated in an aqueous solvent. However, the solvent used for EPD in this study was non-aqueous with the real pa_H related to the measured pH as follows:

$$pa_H = pH - \frac{\Delta Ej}{RT \ln 10 / F} \quad (3)$$

$$\text{or} \quad pa_H = pH - \frac{\Delta Ej}{0.05916} \quad (\text{at } 25^oC) \quad (4)$$

where $pa_H = -\log a_H$ in which a_H is the proton activity in a non-aqueous solvent, ΔEj is the difference between the residual liquid-junction potentials encounter in the standardization and testing step of a standard pH meter (Sarkar & Nicholson, 1996). Wang and Nicholson (1997) calculated $(\Delta Ej/0.05916) = -1.23$ for ethanol suspension.

3.2.2. Effect of applied voltage

The EPD of PZT was performed at pH 4.5-5 with various applied voltages from 50 to 200 V for 1.5 and 2 minutes. The dependence of green films thickness on applied voltage is shown in Figure 5. In general, the thickness increases with an increase in voltage. The maximum green film thickness that could be obtained was approximately 95 µm at 150 V, 2 min. For voltages below 50 V, films deposit too thin unless high electrostatic stability of the suspension is achieved. High applied voltages above 150 V are unfavorable due to the interaction between the as-deposited particles under high driving force. This causes a decrease in green film thickness with a non-uniform surface similar to that described in Figure 4a.

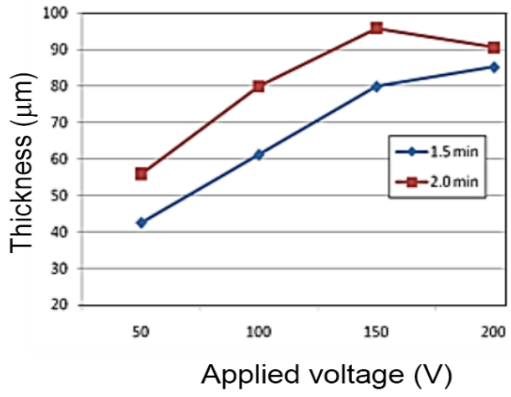

Figure 5. Dependence of the thickness of PZT film on applied voltages at deposition time 1.5 min. and 2 min.

In addition, high applied voltages lead to a high rate of deposition, and the film quality deteriorates drastically due to the flow turbulence of the suspension. Very fast-moving of the particles toward the electrode usually causes a non-closed packing of the film structure because the particles do not have enough time to arrange in the best positions to form a dense structure. Moreover, when

high voltages are applied, the oxidation of the anode occurs, and a change in color of the metal electrode surface was observed during EPD process. As a result, it is more favorable to perform EPD at lower voltage and for a longer time to obtain high-quality films.

3.2.3. Effect of deposition time

Figure 6a describes the dependence of green film thickness on deposition times at three applied voltages, 50, 100 and 150 V. On increasing the deposition time up to 2 minutes, the thickness increases steadily, but then, it decreases when a voltage of higher than 100 V is applied. It can be seen that the film thickness increases quickly with time at high voltages in the early stage, but then, lengthening the deposition time results in a fall of thickness. Meanwhile, although the rise in thickness is relatively slow at as low voltage as 50 V, the thickness was still observed to increase up to 2.5 min or more. It is noted that current intensity falls quickly right after the EPD process starts, corresponding to the rapid deposition of the film. As the film gets thicker, it becomes more resistant to the electric field, hence, the current intensity decreases. The deposition rate therefore decreases as well (Ng & Boccaccini, 2005; Besra & Liu, 2007).

Applied voltage and deposition time are closely correlated since the optimum deposition time can vary with the chosen applied field. For example, the film obtained at an EPD condition of 100 V, 1.5 min. is comparable to that obtained at 50 V, 2 min. Nevertheless, as stated above, it is better to choose a low applied voltage than a high one because the fast deposition rate at high voltages causes porosity. However, a very low voltage may not provide enough electric charge for the particles to move forward the electrode, especially the coarse ones. This will lead to a thinner deposit, as illustrated in figure 6a, which shows a maximum green film thickness of ~ 60 µm at 50 V compared to above 90 µm at 150 V. Consequently, for making the films with reasonable thickness for use, EPD conditions of 150 V, 1.5 min., pH 4.5-5 were applied.

Figure 6b illustrates the thickness of the films sintered at 1,200°C, 1 h from green films deposited at 150 V. The thickness obtained was 80±2 µm for the film deposited in 2 min., which is lower than green film (~ 95 µm) because of the shrinkage of the film when sintering.

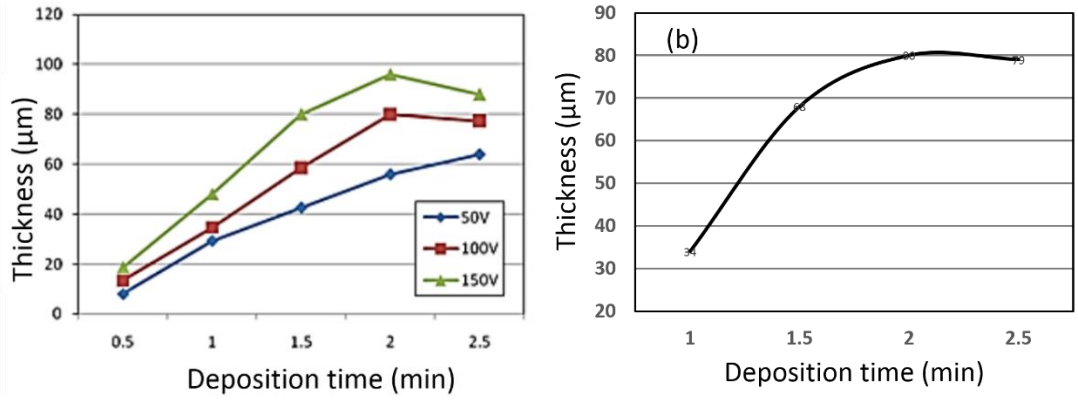

Figure 6. Thickness of PZT films versus deposition time at different constant voltages

(a) Green film at 50 V, 100 V and 150 V

(b) Sintered film at 1,200°C, 1 h from green film deposited at 150 V for 1 to 2.5 min

3.3. Sintering of films

3.3.1. Effect of sintering atmosphere

PZT compositions, when sintered, have been reported to have problems with lead to the loss due to high volatility of PbO (Ng & Boccaccini, 2005; Tassel & Randall, 1999). This causes the change in Pb/Ti and Pb/Zr ratios, but more severely, the perovskite structure of PZT might be distorted or destroyed. In this experiment, PZT films were sintered under an ambient atmosphere with and without a lead-rich powder for comparison. The lead source comprises a 1:0.5:0.5 molar ratio of $PbO:ZrO_2:TiO_2$ with 2% excess PbO. It provides a higher lead vapor pressure so that the loss of PbO is reduced.

Figure 7 presents the XRD traces of PZT films sintered at 1,150°C in lead-rich powder shows the structure of the material is still perovskite while

without the powder, PZT is found to partially decompose into ZrO_2 and the most intense characteristic peak for PZT at 101 is suppressed drastically. It can be seen that the perovskite structure of PZT was almost destroyed, *i.e.*, the composition of the material is no longer single phase PZT. The decomposition into ZrO_2 also occurred in the sample sintered with powder present but to a much lower level. The indexed peaks for the tetragonal perovskite structure of PZT, are in good agreement with the data in both intensities and degrees 2θ.

The morphology image of the film sample sintered at 1,150°C without lead-rich powder is observed to contain a large volume fraction of pores as shown in figure 8a. This is clearly resulted from the lead loss which reduces the density of the film. Meanwhile, the sample covered with lead-rich powder (Figure 8b) shows denser particles and fewer voids. This is confirmed by the XRD patterns in Figure 7c, which indicates the crystal structure is maintained comparable to that of the green film (Figure 7a), except for small ZrO_2 impurity shown at $\bar{1}11$ and 200, whereas figure 7c for the film without lead-rich powder shows a deterioration of the perovskite structure with clear characteristic peaks for TiO_2 and ZrO_2. Therefore, the sintering of PZT materials must be performed in a lead-rich atmosphere to minimize the lead loss and maintain the perovskite structure of PZT.

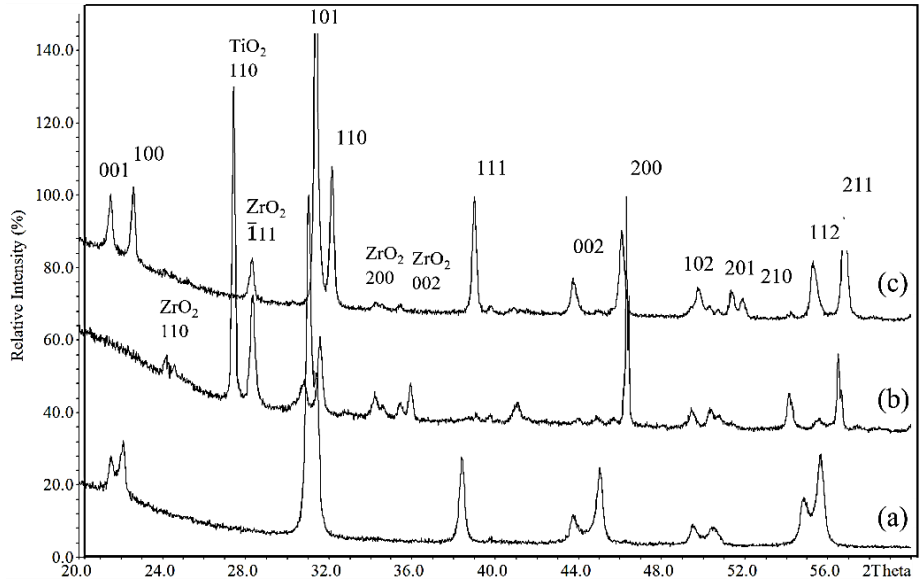

Figure 7. XRD traces of PZT green film (a) and films sintered at 1,150°C without lead-rich powder (b) and with lead-rich powder (c)

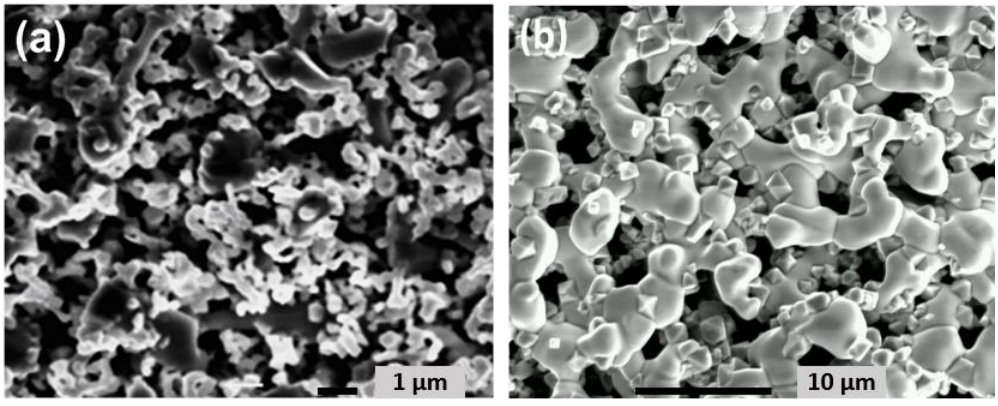

Figure 8. SEM images of the PZT films sintered at 1,150°C without lead-rich powder (a) and with lead-rich powder (b)

3.3.2. Effect of sintering temperatures

PZT films were sintered at various temperatures from 1,100 to 1,250°C with the presence of lead-rich powder. Their XRD patterns are presented in Figure 9. Below 1,100°C, the film structure is quite similar to that of the green film but the material was not well sintered on Pt substrate. The decomposition occurred since ZrO_2 ($\bar{1}11$) and (200) peaks are observed in the traces of sintered film at 1,150°C and above. Obviously, the decomposition also released lead in vapor form. This is interpreted by the separation between the adjacent peaks such as 011 and 110, 101 and 110, 002 and 200, 112 and 211. The more the separation of these couples of peaks, the more the lead loss, and the initial Zr/Ti ratio of 50/50 would gradually fall on increasing temperatures. It should also be noticed that the peaks shift to the right on increasing temperature corresponding with the reduction in Zr/Ti ratio in PZT composition. In other words, there is a tendency of forming Ti-rich PZT and free ZrO_2 phases at increasing temperatures.

The morphologies of PZT films are presented in Figure 10a-d. In all film samples, the SEM images reveal the porous microstructures. Samples at 1,100 and 1,150°C show similar surface microstructures in which the grains connect. The grain size increases in the samples sintered at 1,200 and 1,250°C. It is observed that the structure also contains a great deal of small and large grains together, and small grains seem to increase in number with rising sintering temperatures. While the big grains have smooth surfaces, the small ones are octahedral.

The clear distinction in shape and size between the two types of grains stimulated chemical analysis using EDX. The Zr peak $ZrL\alpha_1$ is at 2.04 keV, PbMα at 2.34 keV and TiMα at 4.51 keV. The compositions of small grains in four samples at different sintering temperatures are quite similar and mainly composed of ZrO_2 which is expressed by the highest intensive peak of Zr at 2.04 keV with a minor Pb composition in 1,100°C sample. EDX spectra for the large grains showed the well-defined peaks of Pb at 2.34 keV in all samples, and Zr and Ti were also detected. It can be inferred that the composition of the large grains is consistent with PZT but the concentration of Zr varies considerably with sintering temperatures. On heating, PZT is decomposed to release free ZrO_2 accompanied with lead loss and a decline in Zr/Ti ratio in the PZT composition. The main PZT phase (large particles) and the secondary phase (small particles) are clearly observed, and it is randomly distributed among the main phase grains. Consequently, the film should be sintered at a low temperature of 1,150°C with lead-rich powder to prevent lead loss in the film.

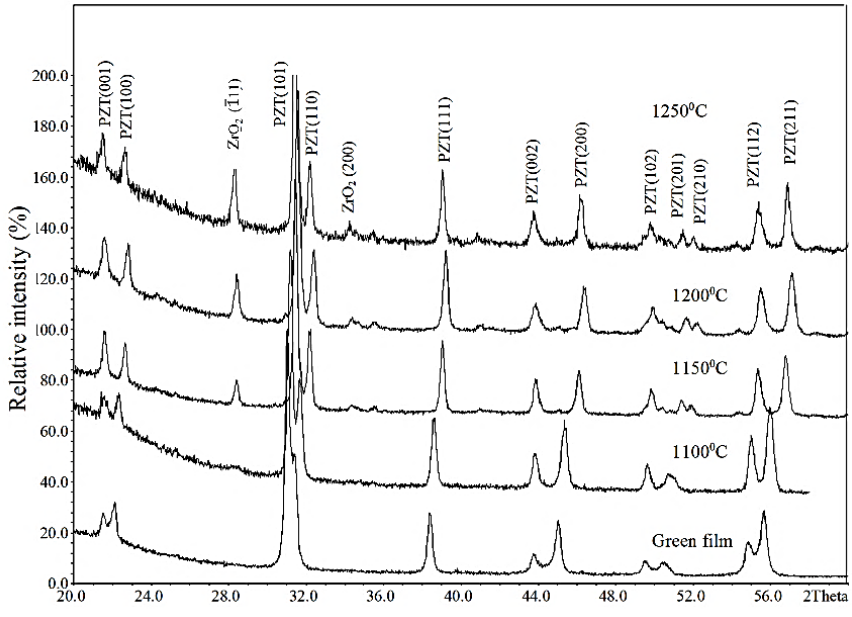

Figure 9. XRD patterns of PZT films sintered at 1,100°C, 1,150°C, 1,200°C and 1,250°C, 4h

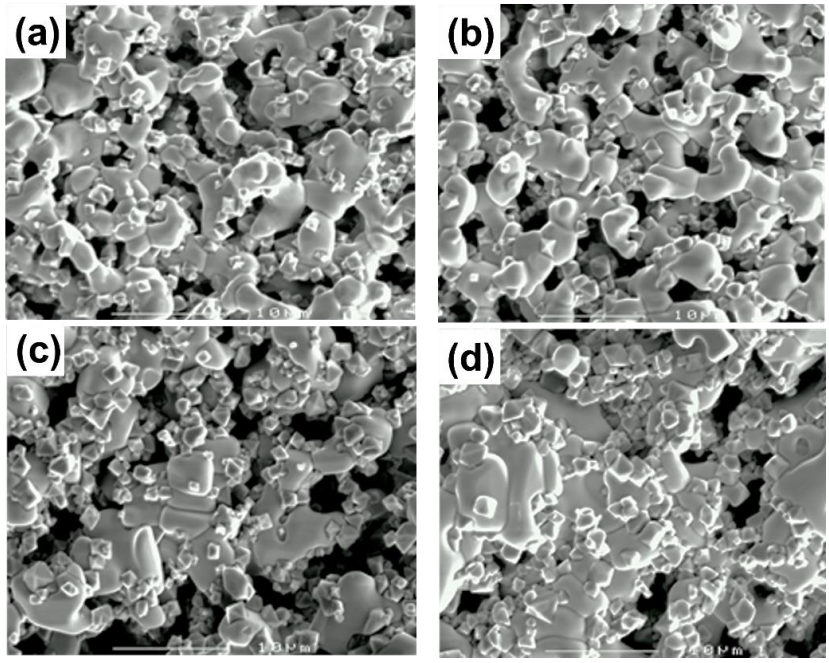

Figure 10. SEM images of PZT thick films sintered at 1,100ºC (a), 1,150ºC (b), 1,200ºC (c) and 1,250ºC (d)

3.4. Electrical measurements

The impedance of PZT film was measured and relative permittivity ε_r (dielectric constant) was calculated as described in equation (1) and (2). At room temperature, the measurement of a film of 68±2 μm thickness, sintered at 1,150ºC resulted in a maximum ε_r of 477±13 at 1 MHz with a loss tangent of 0.089. This value is comparable with other literature (Es-Souni et al., 2005). Figure 11 shows the relative permittivity ε_r plotted as a function of temperature with a frequency of 1 kHz and 1 GHz. The peak at 405ºC indicates the Curie temperature T_C at which a phase transition occurs from tetragonal structure at low temperature end to cubic at high temperatures. At T_C = 405ºC, ε_r reaches ~9,500 for the frequency 1 GHz and ~ 18,000 at 1 kHz. T_C for PZT in this study is a little higher than reported T_C for the composition PZT 50/50, showing the fabricated film composition is on the Ti-rich end as discussed above. PZT-based ceramics are virtually among the best dielectric materials with a highest dielectric constant compared with that of other dielectric ceramics such as $BaTiO_3$ (ε_r~ 6,000 at 1 kHz), $PbTiO_3$ (1,100 at 1KHz) (Yusoff et al., 2020; Chaudhari & Bichile, 2013).

4. CONCLUSIONS

In this study, PZT 50/50 powder was fabricated by calcinating a PbO, ZrO_2 and TiO_2 mixture with 2% excess PbO at 950ºC, 4 h. XRD analysis showed that the resulting composition was single phase with a typical tetragonal perovskite structure. No trace of PbO was detected. The calcined powder was attrition milled and the average particle size was ~2 μm.

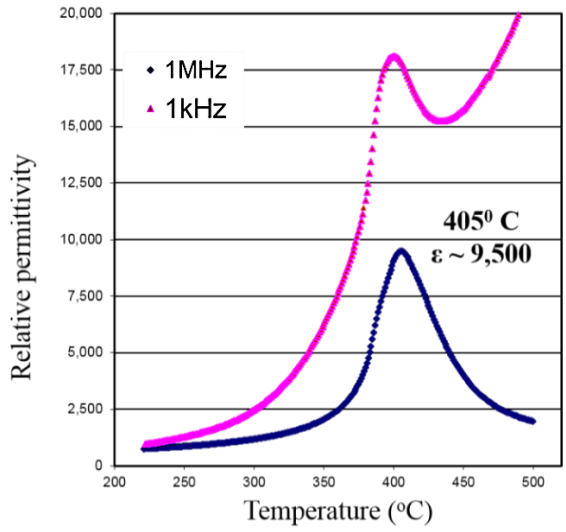

Figure 11. Relative permittivity vs. temperature of PZT sintered at 1,150°C, 1kHz and 1 MHz

PZT green film was deposited by EPD process onto Pt substrate at pH 4.5-5 with ethanol as the solvent. An optimum condition for EPD was found to be 150 V, 1.5 min. A maximum PZT green film thickness of 95 µm was achieved. Meanwhile, sintered PZT film had a maximum thickness of 80 ±2µm. PZT compositions had to be sintered in a lead-rich atmosphere to minimize the decomposition of the film. Without a lead-rich atmosphere, Zr/Ti ratio declined and free ZrO_2 occurred when increasing sintering temperatures. SEM and EDX revealed a two-phase microstructure composed of small ZrO_2 particles and the main PZT phase. Therefore, films should be sintered at a low temperature of 1,150°C to prevent secondary phase formation.

At room temperature and 1MHz, the PZT thick film sintered at 1,150°C had a relative permittivity ε_r of 477± 13, $tan\delta$ of 0.089 while ε_r reached ~9,500 at T_C ~ 405°C, which are typical for a dielectric ceramic. The fabricated thick PZT films are promising for application in microactuators.

ACKNOWLEDGMENT

The authors thank the Vietnam Ministry of Education and Training for financial support to this research (Grant 322).

REFERENCES

Besra, L. & Liu, M. (2007). A review on fundamentals and applications of electrophoretic deposition (EPD). *Progress in Materials Science, 52*(1), 1-61. https://doi.org/10.1016/j.pmatsci.2006.07.001

Carter, C. B. & Norton, M. G. (2013). *Ceramic Materials: Science and Engineering*. Springer, 2nd Edition.

Chaudhari, V. A. & Bichile, G. K. (2013). *Smart Materials Research*. Synthesis, Structural, and Electrical Properties of Pure $PbTiO_3$ Ferroelectric Ceramics, 2013, 147524. http://dx.doi.org/10.1155/2013/147524

Doungdaw, S., Uchikoshi, T., Noguchi, Y., Eamchotchawalit, C., & Sakka, Y. (2005). Electrophoretic deposition of lead zirconate titanate (PZT) powder from ethanol suspension prepared with phosphate ester. *Science and Technology of advanced materials*, *6*(8), 927. https://doi.org/10.1016/j.stam.2005.09.002

Es-Souni, M., Kuhnke, M., Piorra, A. & Solterbeck, C. H. (2005). Pyroelectric and piezoelectric properties of thick PZT films produced by a new sol–gel route. *Journal of the European Ceramic Society, 25*(12), 2499–2503. https://doi.org/10.1016/j.jeurceramsoc.2005.03.090

Frantti, J., Lappalainen, J., Eriksson, S., Lantto, V., Nishio, S., Kakihana, M., Ivanov, S. and Rundlöf, H. (2000). Neutron diffraction studies of $Pb(Zr_xTi_{1-x})O_3$ ceramics. Japanese Journal of Applied Physics, ***39***(9B) 5697. https://doi.org/10.1143/jjap.39.5697

Hata, T., Kawagoe, S., Zhang, W., Sasaki, K. & Yoshioka, Y. (1998). Proposal of new mixture target for PZT thin films by reactive sputtering. *Vacuum, 51*, 665–671.

Hsu, Y. C., Wu, C. C., Lee, C. C., Cao, G. Z. & Shen, I. Y. (2004). Demonstration and characterization of PZT thin film sensor and actuators for meso- and micro-structures. *Sensors and Actuators A: Physical,*

116(3), 369–377. https://doi.org/10.1016/j.sna.2004.05.024

Jaffe, B., Cook, W. R. & Jaffe, H. (1971). *Piezoelectric Ceramics*. Academic Press, London.

Jun, B. S. & Joo, H. K. (2008). Suspension stability of $Pb(Zr_{0.58}\ TiO_{0.42})O_3$ nano-particles during electrophoretic deposition. *Journal of Physics and Chemistry of Solids, 69*(5,6), 1330-1333. https://doi.org/10.1016/j.jpcs.2007.10.130

Kalinina, E. G. & Pikalova, E. Y. (2019). New trends in the development of electrophoretic deposition method in the solid oxide fuel cell technology: theoretical approaches, experimental solutions and development prospects. *Russian Chemical Reviews, 88*(12), 1179-1219.

Kuepper, H., Leuerer, T., Schnakenberg, U., Mokwa, W., Hoffmann, M., Schneller, T., Boettger, U. & Waser, R. (2002). PZT thin film for piezoelectric microactuator applications. *Sensors and Actuators A, 97-98*, 680–684.

Lee, B. Y., Cheon C., Kim, J. S., Bang, K. S. B., Kim, J. C. & Lee, H. G. (2002). Low Temperature Firing of PZT Thick Films Prepared by Screen Printing Method. *Materials Letters, 56*(4), 518-521. https://doi.org/10.1016/S0167-577X(02)00543-8

Ma, J. & Cheng, W. (2002). Deposition and packing study of sub-micron PZT ceramics using electrophoretic deposition *Materials Letters, 56*, 721-727. https://doi.org/10.1016/S0167-577X(02)00602-X

Ma, J., Zhang, R., Liang, C.H. & Weng, L. (2003). Colloidal characterization and electrophoretic deposition of PZT, *Materials Letters, 57*, 4648–4654. https://doi.org/10.1023/a:1025092506583

Mikeska, T. & Cannon, W. R. (1988). Non-aqueous dispersion properties of pure barium titanate for tape casting. *Colloids and Surfaces, 29*(3), 305–321. https://doi.org/10.1016/0166-6622(88)80125-2

Miyazawa, K., Ito, K. & Maeda, R. (2000). Structure and electrical properties of multilayer PZT films prepared by sol–gel processing. *Ceramics International, 26*(5), 501–506. https://doi.org/10.1016/S0272-8842(99)00085-1

Mills, S. C., Smith, C.S., Arnold, D. P. & Andrew, J. S. (2020). Electrophoretic deposition of iron oxide nanoparticles to achieve thick nickel/iron oxide magnetic nanocomposite films. *AIP Advances, 10*(1), 015308. https://doi.org/10.1063/1.5129797

Mittal, G. & Rhee, K. Y. (2021). Electrophoretic deposition of graphene on basalt fiber for composite applications. *Nanotechnology Reviews, 10*(1), 158-165. https://doi.org/10.1515/ntrev-2021-0011

Moulson, A. J. & Herbert, J. M. (2003). *Electroceramics*. John Wiley & Son, Sussex.

Ng, S. Y. & Boccaccini, A. R. (2005). Lead zirconate titanate films on metallic substrates by electrophoretic deposition. *Material Science and Engineering B, 116*, 208-214. https://doi.org/10.1016/j.mseb.2004.10.013

Piticescu, R. M., Moisin, A. M., Taloi, D., Badilita, V. & Soare, I. (2004). Hydrothermal synthesis of ultradisperse PZT powders for polar ceramics. *Journal of the European Ceramic Society, 24*, 931–935. https://doi.org/10.1016/S0955-2219(03)00545-4

Rehman, M. A. U., Chen, Q., Braem A., Shaffer, M. S. P. & Boccaccini, A. R. (2021). Electrophoretic deposition of carbon nanotubes: recent progress and remaining challenges. *International Materials Reviews. 66(8), 533-562.* https://doi.org/10.1080/09506608.2020.1831299

Sarkar, P. & Nicholson, P. S. (1996). Electrophoretic deposition (EPD): Mechanisms, kinetics, and application to ceramics. *Journal of American Ceramic Society, 79*, 1987–2002. https://doi.org/10.1111/j.1151-2916.1996.tb08929.x

Setter, N. (2001). Electroceramics: looking ahead. *Journal of the European Ceramic Society, 21*, 1279-1293. https://doi.org/10.1016/S0955-2219(01)00217-5

Szklarska, M., Losiewicz, B., Dercz, G., Maszybrocka, J., M., Marzena, Baron, M. R., Stach, S. (2020). Electrophoretic deposition of chitosan coatings on the Ti15Mo biomedical alloy from a citric acid solution. RSC Advance**, *23***, 13386-13393. https://doi.org/10.1039/D0RA01481H

Tassel, J.V. & Randall, C.A. (1999). Electrodeposition and sintering of thin/thick PZT films. *Journal of European Ceramic Society, 19*, 955-958. https://doi.org/10.1016/S0955-2219(98)00352-5

Wang, G., Sakar, P. & Nicholson, P. S. (1997). Influence of acidity on the electrostatic stability of alumina suspensions in ethanol. *Journal of the American Ceramic Society, 80*(4), 965-972.https://doi.org/10.1111/j.1151-2916.1997.tb02928.x

Wu, A. & Vilarinho, P. M. (2006). Electrophoretic Deposition of Lead Zirconate Titanate films on Metal Foils for Embedded components. *Journal of the American Ceramic Society, 89*(2), 575-586. https://doi.org/10.1111/j.1551-2916.2005.00732.x

Yusoff, N. H., Osman, R.A.M., Idris, M.S., Muhsen, K. N., Nor & N. I. M. (2020). Dielectric and structural analysis of hexagonal and tetragonal phase $BaTiO_3$. *AIP Conference Proceedings.* **2203**, 020038. https://doi.org/10.1063/1.5142130